THE MASAR PROJECT: DESIGN AND DEVELOPMENT

V. C. Koo, Y. K. Chan, G. Vetharatnam, T. S. Lim
B. K. Chung, and H. T. Chuah

Faculty of Engineering & Technology
Multimedia University
Jalan Ayer Keroh Lama, Bukit Beruang
75450 Melaka, Malaysia

Abstract—In 2002, the MASAR (Malaysian Airborne Synthetic Aperture Radar) project was initiated at Multimedia University (MMU), in collaboration with the Malaysian Centre for Remote Sensing (MACRES). The main objective of this project is to construct an instrument for earth resource monitoring in Malaysia. The proposed SAR system is a C-band, single polarization, linear FM radar. This paper outlines the major design issues and considerations for MASAR. In particular, the design and construction of the microwave system, microstrip antenna, and a high-speed data recording system are described. The SAR processing algorithm which incorporates motion compensation capability for high resolution image generation is also outlined.

1. INTRODUCTION

Radar has long been used for military and commercial purposes in a wide variety of applications such as imaging, guidance, remote sensing and global positioning [1]. The use of SAR for remote sensing is particularly suited for tropical country such as Malaysia. By proper selection of operating frequency, the microwave signal can penetrate clouds, haze, rain precipitation with very little attenuation, thus allowing operation in unfavorable weather condition that preclude the use of visible-light/infrared system [2]. For national monitoring and management of earth resources, limited number and untimely supply of the required SAR images have been a major problem. Therefore the need for developing our own SAR technology and sensor system is apparent.

The MASAR project started in 2002, after preparatory studies in the previous years [3]. The proposed system is an airborne, single polarization, linear FM radar operating at C-band. This SAR system is designed to operate at moderate altitudes with low transmit power and small swath width in order to optimize the development cost and operating cost. It will serve as a test-bed for demonstrating SAR technology and acquiring data for the development of radar processing techniques and applications.

This paper is organized as follows. Section 2 outlines the major design issues and considerations for MASAR. A computer-based SAR simulator is developed to provide better understanding of the interaction between various design parameters. It also serves as a platform to validate the SAR image formation and motion compensation algorithms. Section 3 describes the development of various SAR subsystems including the microstrip patch antenna, the radar electronics, and the high-speed data acquisition system. A challenge in airborne SAR system development involves compensation for nonlinear platform motion that introduces phase distortion in SAR raw data. Section 4 focuses on the effects of platform motion errors. The SAR processing algorithm, which incorporates motion compensation, is presented. Finally, Section 5 concludes the paper.

2. DESIGN CONSIDERATIONS

2.1. System-Level Requirements

2.1.1. Operating Frequency

C-band (4–8 GHz) frequency is widely used for high-resolution land imaging, agricultural monitoring and ocean observations. In this frequency band, incident wave tends to be reflected more by vegetation canopies rather than the surface layer. This penetration characteristic allows the canopy biomass and soil below the canopy to be analyzed. The center frequency of the MASAR is selected at 5.3 GHz, which is within the allowable spectrum (5250–5460 MHz) defined by International Telecommunication Union (ITU) for Earth Exploration Satellite System (EESS) [4]. Beside the reason of having low absorption in the atmospheric-window region, the size of a C-band antenna is considerably small and most of the RF components are easily available.

2.1.2. Modulations

In radar system, there are basically three types of widely used modulation schemes: pulse, linear FM (LFM) chirp, and phase coded. As compared to a pulse system, the same average transmitting power can be achieved with lower peak amplitude in a typical LFM system. The LFM configuration is employed in this project since it gives better sensitivity without sacrificing range resolution. It allows for the use of commercially available microwave components that have moderate peak power handling capability.

2.1.3. Mode of Operation

The two most common SAR imaging modes are stripmap and spotlight. The stripmap is standard mode of SAR operation, widely used by airborne SAR sensors where a strip (swath) to the side of the aircraft is imaged. On the other hand, a spotlight SAR steers its antenna beam to continuously illuminate a specific terrain patch during data collection. The spotlight mode is suitable to collect fine-resolution data from localized areas, while the stripmap mode is more efficient when used for coarse-resolution mapping of large regions. In our design, the stripmap mode is the preferred choice.

2.1.4. Polarization

Single polarization mode is proposed for simple classification and multi-temporal change detection. VV-polarization is the preferred configuration since it is sensitive to the vegetation's vertical canopy structure, thus providing the opportunity for crop type and growth stage discrimination.

2.1.5. Dynamic Range

Base on the measurement results reported in numerous literatures, it is found that the typical value of scattering coefficients for various categories of terrain falls in the range from $0\,\text{dB}$ to $-30\,\text{dB}$ [5]. Therefore, a wide dynamic range ($>30\,\text{dB}$) is needed to accommodate the measurement of various types of terrain.

2.1.6. Resolution

Typical resolution of airborne SAR ranges from $1\,\text{m}$ to $20\,\text{m}$ [6]. It depends mostly on the application requirements. Since the main objective is to establish our own airborne SAR with capability of monitoring earth resources, resolution of $8 \times 8\,\text{m}$ for both range and azimuth direction will be adequate.

2.1.7. Incident Angle

The MASAR will be operated at incident angle of $50°$. This is due to the fact that backscattering coefficients of natural targets such as soil, grass and vegetation are maintained almost constant over the incident angle of $40°$ to $60°$ [5].

2.1.8. Antenna Requirements

A planar, lightweight, small size, linearly polarized microstrip patch array panel is proposed. The center frequency for the array is set at 5.3 GHz, with more than 40 MHz bandwidth. The directive gain of the panel should be more than 18 dBi for good detection in the presence of noise.

2.1.9. Signal Processor

The on-board facility consists of a high-speed analog-to-digital converter, a front-end processor, and a high-density digital data recorder to store the raw data. The SAR images will be produced by ground processing facility. Motion compensation and auto-focusing technique would be applied to improve image resolution and quality.

2.1.10. Airborne Platform

A small (executive type) jet aircraft will be used to install the radar system. The radar system shall support true ground speed up to 100 m/s and operating altitude at about 7500 m to avoid the low altitude turbulence in the troposphere. A pressurized aircraft is needed to overcome the reduced levels of oxygen. The aircraft suggested shall have 6 to 12 passenger seats to provide enough cabin space for the payload.

2.1.11. Others

The development and operating costs of the MASAR should be kept as low as possible.

2.2. Design Parameters Selection

Traditionally, design and development of SAR systems have been expensive and time-consuming tasks. The design process often requires extensive redesign of hardware and software to optimize system performance. It is thus essential to carry out a proper SAR simulation before the actual implementation of the hardware system. Great efforts have been carried out by many institutions in the development of their own in-house SAR simulators for mission planning, terrain modeling, algorithm testing, and as a tool for understanding SAR process [7–9].

A complete simulator would model end-to-end SAR process, including the sensor-target geometry, the antenna and receiver systems, the operation of a signal processor, and the production of radar
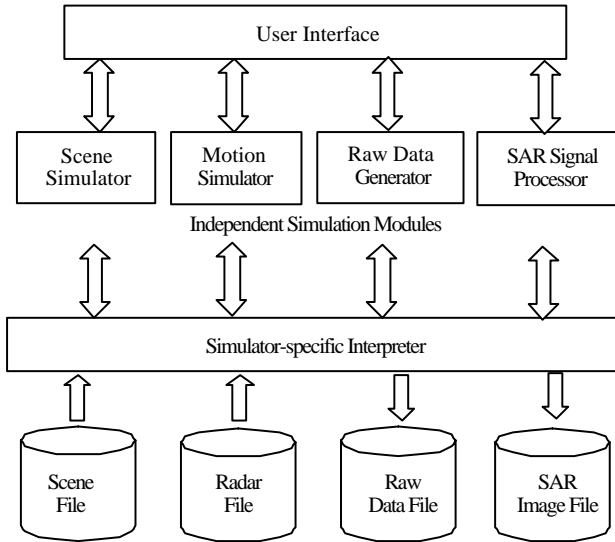
Figure 1. Block diagram of a modular-based SAR simulator.

image. As illustrated in Fig. 1, we have developed a modular-based simulator that consists of various independent modules sharing a pool of data files. Each module may be developed and executed separately, depending on individual applications. The target response, platform geometry and radar parameters are the inputs, while the raw data and basic SAR image are computed through an internal SAR processor as outputs.

The simulator is implemented using Matlab® software. The first step is to create a complex reflectivity map of the scene to be imaged. Typically, the scene is modeled as a collection of independent random scatterers per resolution element by taking into consideration the electromagnetic characteristics, terrain model, geometric distortions, speckle effects, and masking phenomena. The effects of antenna pattern, sensor characteristics and radar flight path information are included to compute the SAR raw signal. In the subsequent step, the raw data is used to produce a SAR image on the slant range plane projections. The last step involves various post processing operations such as slant-range to ground range projection, resampling and gray levels equalization.

Based on the system-level requirements described in Section 2.1, the design parameters are iteratively selected and the results are evaluated using the SAR simulator. Table 1 presents the selected system parameters for the MASAR system.

Table 1. The MASAR specifications.

System Parameter	Specification
Mode of operation	Stripmap
Operating frequency, f_c	5.3GHz (C-band)
Bandwidth, B	20MHz
Chirp pulse duration, τ_p	20µs
Pulse repetition frequency	1000 HZ
Transmitter peak power, P_t	100W
Polarization	Linear, VV
Antenna gain, G	>18dBi
Elevation beamwidth, β_{el}	24°
Azimuth beamwidth, β_{az}	3°
Synthetic Aperture Length,	~200m
ADC sampling frequency,	100MHz
ADC quantization	12-bit
Data rate, d_r	100Mbps
Recorder capacity	2x160GB, SATA
Data take duration, T_d	>5 hour
$\sigma°$ dynamic range	0 dB to -30 dB
Singal-to-noise ration, SNR	>10dB
Best slant range resolution,	7.5 m
Best azimuth reoslution, ρ_a	7.5 m (2-looks)
Incident angle, θ	50°
Swath width, W	~8km
Platform height, h	7500 m
Nominal platform speed, v_0	100 m/s
Operating platform	Pressurized aircraft

3. SYSTEM IMPLEMENTATION

The functional block diagram of the MASAR system is shown in Fig. 2. The system is based on a low-IF design. It consists of a microstrip antenna, a radar electronics subsystem and a data acquisition system.

3.1. Antenna

A probe fed rectangular patch antenna is developed for the MASAR system. Patch antennas are relatively easy to fabricate and low cost. At the operating frequency of 5.3 GHz, the patch has a dimension of 19.0 mm × 15.4 mm. The signal distribution network (feed transmission
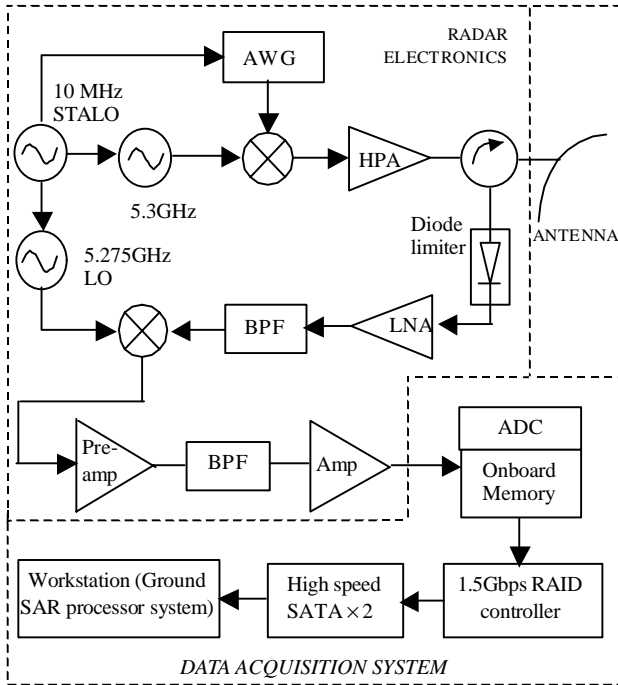
Figure 2. System block diagram of MASAR.

line) is placed behind the ground plane to reduce spurious feed radiation. The impedance of the patch and its transmission line is matched at $50\,\Omega$ by feeding the patch at $4.5\,\mathrm{mm}$ offset from the edge.

The radiation pattern of the array is designed based on several factors associated with an airborne SAR system [10]. The prominent factors are the azimuth ambiguity, slant-range variations and reflections. In the azimuth plane (or H-plane), a narrow pencil-beam with $3°$ beamwidth is designed, with the sidelobes suppressed by $30\,\mathrm{dB}$. Sidelobe suppression is necessary due to azimuth ambiguity effects. The H-plane radiation pattern is realized using Dolph-Chebyshev array distribution [11]. To achieve the required beamwidth and sidelobe suppression, a 28-element linear array spaced at 0.74λ are required. The amplitude distribution of the array is shown in Table 2. The array factor of the 28-element linear array is shown in Fig. 3. The total radiation pattern is the product of this array factor and the radiation pattern of the patch. Thus, the sidelobes near the end-fire are suppressed.

In the elevation plane (or E-plane), a cosec-squared shaped-beam

Table 2. Dolph-Chebyshev array excitation coefficients.

Element no.	1	2	3	4	5	6	7
Excitation coefficient	1.37	0.86	1.10	1.36	1.63	1.91	2.19
Element no.	8	9	10	11	12	13	14
Excitation coefficient	2.45	2.70	2.92	3.11	3.25	3.35	3.41

Table 3. E-plane excitation coefficients.

Element no.	1	2	3	4	5
Magnitude	2.40	3.82	2.89	0.66	1.00
Phase (deg.)	-164	-161	-156	-120	0
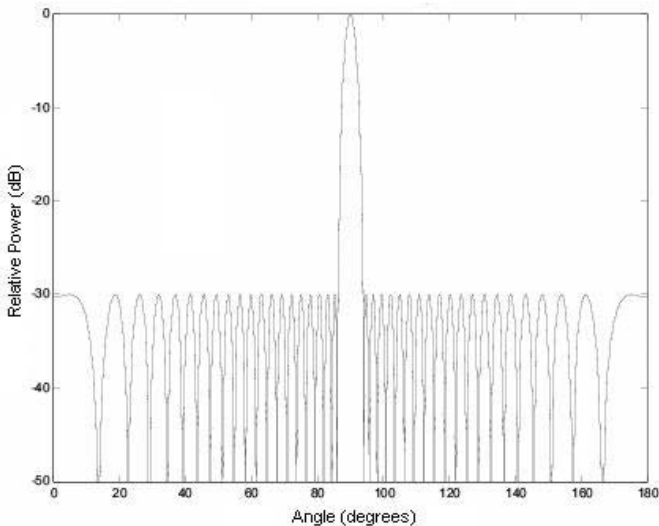
Figure 3. H-plane array factor pattern.

pattern is proposed for angular sector $76°$ to $100°$, which constitutes the main beam, while the sidelobes are suppressed by $15\,\mathrm{dB}$ to avoid reflections from aircraft structure. Utilizing Elliott synthesis method [12], a 5-element array spaced at 0.7λ is designed for the E-plane. The excitation coefficients are tabulated in Table 3. The array factor for the E-plane is shown in Fig. 4.

The planar array is constructed by combining the linear E-plane and H-plane arrays. The effect of the element pattern must be considered in the E- and H-plane patterns before fabricating the array.
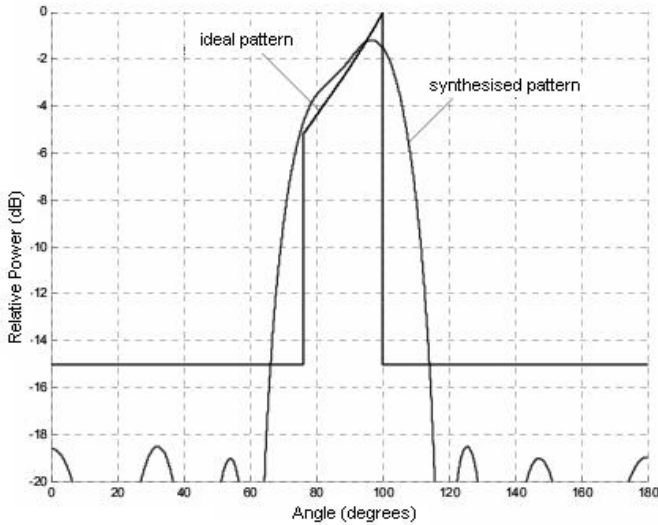
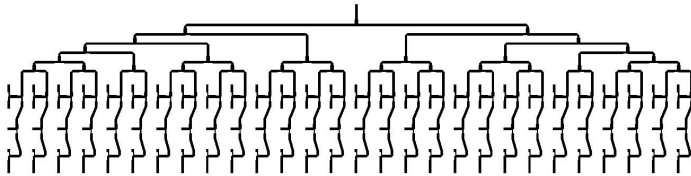**Figure 4.** *E*-plane array factor pattern.

Figure 5. Signal distribution network for the antenna array.

In total, 140 patches are required for the array. The combined signal distribution network for the array is shown in Fig. 5.

3.2. Radar Electronics

The microwave source is a 5.3 GHz dielectric resonator oscillator (DRO) that locks to a 10 MHz stable local oscillator (STALO). An arbitrary waveform generator (AWG) is used to generate the required LFM chirp signal. The output of the up-converter mixer is routed to a solid-state high power amplifier with 40 dB gain. The amplified signal is then radiated through the antenna via a circulator. The transmitted waveform is centered at 5.3 GHz with 40 MHz bandwidth.

The first stage of the receiver is a +20 dBm PIN diode limiter. Followings are a low noise amplifier (LNA) with a noise figure of

1.6 dB and a band-pass filter. The down-converted mixer is used to convert the received signal to an intermediate frequency (IF) centered at 25 MHz. The local oscillator signal is phase-locked to 10 MHz STALO to preserve the coherency of received signal. The main function of the IF section is to filter and amplify the IF signal from the mixer. The IF band-pass filter is designed to operate from 5 MHz to 45 MHz. A prototype RF transceiver has been developed, where both range detection and radar cross section (RCS) measurement capabilities are verified in the field experiments [13].

3.3. Data Acquisition System

The MASAR employs a PC-based digital signal processing system for data acquisition. It consists of a 12-bits 100 MHz analogue-to-digital converter (ADC). The ADC is capable of converting the down-converted SAR echoes into digital signals and stores them into an on-board memory bank.

High-speed raw data recorder is the key component of the airborne SAR system. It must reliably record the real-time SAR data without loss. The recorder consists of a Redundant Array of Independent Disks (RAID) adapter and two serial ATA (SATA) 160 GB hard disks. RAID is a method of combining several hard disks (physical disks) into one logical unit (logical disk). Such combination can offer either fault tolerance or higher data throughput than a single hard disk system. The RAID level used in the MASAR system is RAID 0/1, which incorporates highest performance with data protection.

The recorder receives raw data from ADC and records on SATA at a rate of 100 Mbit per second. All the stored data are then transferred to a ground processing system for SAR imaging and post-processing. The ground processing system is a high-end general-purpose workstation with 2.4 GHz processor and 1 Gbyte memory. The SAR image formation procedures are described in the next section.

4. SAR IMAGE FORMATION

4.1. System Model

Consider a stripmap SAR system that travels along y-direction (cross-range) at a nominal altitude, h. As shown in Fig. 6, the platform trajectory is subject to three-dimensional deviations from an ideal straight-line path. The x-coordinate is used to identify ground-range, while z specifies the altitude domain in three-dimensional geometry. As the aircraft is flown, the radar antenna forms the required elements in the synthetic array. The aircraft's nominal speed is v_0 and the
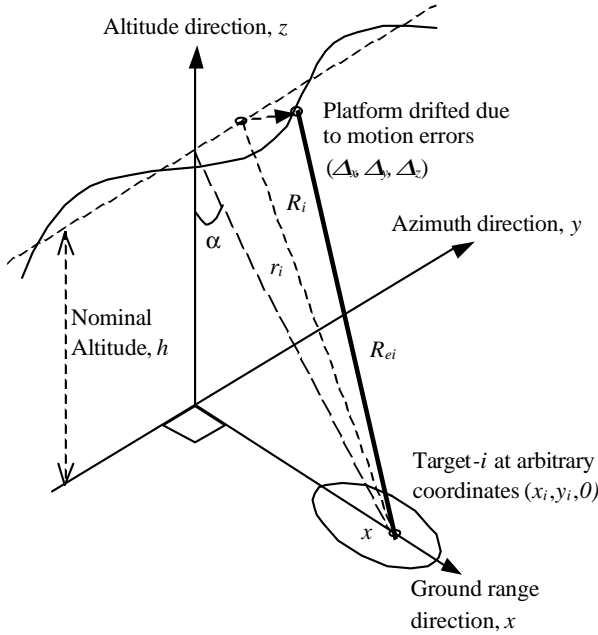
Figure 6. The SAR geometry.

synthetic aperture length that formed over time interval T is L_{syn}. The surrounding medium is assumed to be homogeneous with wave propagation speed c.

We denote the actual vehicle trajectory in the spatial measurement domain as a function of the cross-range domain via

$$\lfloor \Delta_x(y), y + \Delta_y(y), \Delta_z(y) + h \rfloor \tag{1}$$

where $\Delta_x(y), \Delta_y(y)$ and $\Delta_z(y)$ are, respectively, the motion errors in the x-, y-, and z-directions. Let

$$\Delta_r(y) = \Delta_x(y) \sin \alpha - \Delta_z(y) \cos \alpha \tag{2}$$

be the projection of the x- and z-directionmotion errors onto the slant range plane. The uncompensated slant range for a point target-i located at coordinates $(x_i, y_i, 0)$ is given by

$$R_{ei}(y) = \sqrt{(r_i - \Delta_r(y))^2 + (y - y_i + \Delta_y(y))^2} \tag{3}$$

where

$$r_i = \sqrt{x_i^2 + h^2} \tag{4}$$

At each of the cross-range position, y, the radar radiates a burst of transmit signal, $p(t)$, to the target under illumination. In the presence of motion errors, the uncompensated echoed signal (or raw data) measured at time t can be written in terms of target reflectivity function $f(r_i, y_i)$ as

$$s_e(t, y) = \iint_i f(r_i, y_i) p(t - 2R_{ei}/c) dr_i dy_i \tag{5}$$

The Fourier Transform of the $s_e(t, y)$ with resect to t-domain is given by

$$S_e(\omega, y) = \iint f(r_i, y_i) P(\omega) e^{-j2kR_i} e^{-j\phi_e(y)} dr_i dy_i \tag{6}$$

where

$$\phi_e(y) = 2k(R_i - R_{ei}) \tag{7}$$

$k = \omega/c$ is the wavenumber and $P(\omega)$ is the Fourier Transform of $p(t)$.

As suggested by (6), the effects of motion errors introduce multiplicative phase errors $\phi_e(y)$ on the measured SAR signal in the (ω, y) domain. The phase errors modulate the target signal with the tendency to degrade SAR image quality. Taking into consideration the effects of additive noise, $n_s(\omega, y)$, we shall model the SAR azimuth channel as

$$S_e(\omega, y) = \hat{S}(\omega, y) e^{j\phi_n(y)} + n_s(\omega, y) \tag{8}$$

where $\hat{S}(\omega, y)$ is the error-free echoed signal to be recovered.

4.2. SAR Image Formation

The origin of the SAR image formation described below can be found in the wave equation inversion theory [14], which is also referred as wavefront reconstruction theory or holography [15]. Various implementation algorithms that based on the wavefront reconstruction theory have been proposed and discussed by Soumekh [16]. In MASAR, the image formation is based on a parallel implementation of the wavefront reconstruction theory, known as the range-stacking algorithm. The range-stacking algorithm does not require interpolation, and thus it does not suffer from the truncation errors. It is possible to implement this algorithm using parallel processors for real-time processing. Furthermore, the motion compensation can easily be integrated into the algorithm.

Fig. 7 shows the simplified block diagram of the SAR image formation algorithm. The reconstruction equation for range bin r_n
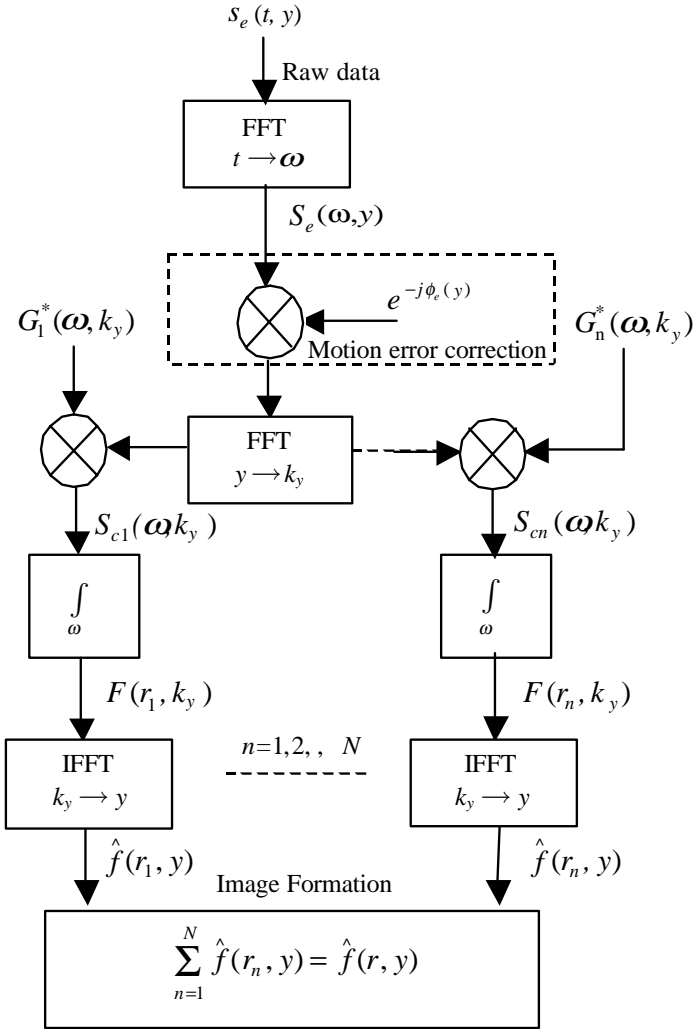
$s_e(t, y)$

Raw data

FFT
$t \rightarrow \boldsymbol{\omega}$

$S_e(\omega, y)$

$G_1^*(\boldsymbol{\omega}, k_y)$ $e^{-j\phi_e(y)}$ $G_n^*(\boldsymbol{\omega}, k_y)$

Motion error correction

FFT
$y \rightarrow k_y$

$S_{c1}(\boldsymbol{\omega}, k_y)$ $S_{cn}(\boldsymbol{\omega}, k_y)$

$\int\limits_{\omega}$ $\int\limits_{\omega}$

$F(r_1, k_y)$ $F(r_n, k_y)$

$n=1,2,,\ N$

IFFT
$k_y \rightarrow y$ IFFT
$k_y \rightarrow y$

$\hat{f}(r_1, y)$ $\hat{f}(r_n, y)$

Image Formation

$$\sum_{n=1}^{N} \hat{f}(r_n, y) = \hat{f}(r, y)$$

Figure 7. The MASAR image formation algorithm.

may be written as

$$\hat{f}(r_n, y) = \int\limits_{k_y} \left[\int\limits_{\omega} S(\omega, k_y) G_n^*(\omega, k_y) d\omega \right] e^{jk_y y} dk_y \qquad (9)$$

where k_y is the spatial frequency for y-domain, and $G_n(\omega, k_y)$ is the

reference signal generated for range bin r_n:

$$g_n(t, y) = p\left(t - 2\sqrt{r_n^2 + y^2}/c\right) \tag{10}$$

This process is repeated for each range bin r_n for $n = 1, 2, \ldots, N$, to obtain a two-dimensional SAR image:

$$\hat{f}(r, y) = \sum_{n=1}^{N} \hat{f}(r_n, y) \tag{11}$$

In this implementation, the two-dimensional SAR data is separated into n-array of azimuth data. Therefore, it is possible to perform one-dimensional motion compensation and processing for each range bin, as discussed in the following section.

4.3. Motion Analysis and Compensation

Errors in aircraft motion are mainly due to atmospheric disturbances and intentional maneuver. Typically, these variations are very slow as compared to the illumination time, T. The resulting phase perturbations may be approximated by the first few terms of a Taylor series expansion relative to the center of the processing aperture:

$$\phi_e(y) = c_0 + c_1 y + c_2 y^2 + \cdots \qquad y \in [0, L_{syn}] \tag{12}$$

Since the SAR processing is not affected by a constant phase error, the coefficient c_0 shall be omitted in the following discussions. Lets denote the uncompensated velocities and accelerations in the cross range and slant range domains as (v_c, a_c) and (v_r, a_r), respectively. Expanding (3) in a Maclaurin series and assuming the deviations are small, we get,

$$R_{ei}(y) \approx r_i - \varepsilon_{\dot{r}} y + \frac{1}{2r_i}[(1 + \varepsilon_{\dot{c}})^2 - \varepsilon_{\ddot{r}}]y^2 \quad y \in [0, L_{syn}] \tag{13}$$

where the normalized motion coefficients are defined as [17]:

$$\varepsilon_{\dot{r}} = \frac{v_r}{v_o} \quad \text{(normalized slant-range velocity)} \tag{14}$$

$$\varepsilon_{\ddot{r}} = \frac{a_r v_i}{v_o^2} \quad \text{(normalized slant-range acceleration)} \tag{15}$$

$$\varepsilon_{\dot{c}} = \frac{v_c}{v_o} \quad \text{(normalized cross-range velocity)} \tag{16}$$

Comparing (7), (12) and (13), we have the following phase error coefficients:

$$c_1 = -2k\varepsilon_{\dot{r}} \quad \text{(linear term)} \tag{17}$$

$$c_2 = \frac{k}{r_i}[(1 + \varepsilon_{\dot{c}})^2 - \varepsilon_{\ddot{r}} - 1] \quad \text{(quadratic term)} \tag{18}$$

The linear phase error introduces a factor $e^{jc_1 y}$ in the integrand of (6) which causes a displacement in the image relative to the case when $c_1 = 0$. If the linear coefficient is space-invariant, the effect is a displacement of the entire scene — such errors are generally not of interest. However, if the coefficient varies across the aperture position, the relative spatial locations within the image will be distorted. In order to keep the geometry distortion on a scale of one-half of the image resolution, the motion error should not move through more than one range resolution cell across the synthetic length L_{syn}, i.e.,

$$|c_1 L_{syn}| < 2k\rho_r \tag{19}$$

The more severe phase error is, of course, due to the quadratic term, c_2. Multiplication by $e^{jc_2 y^2}$ term before Fourier Transform processing causes defocusing of the system impulse response. The output image will be smeared and defocused due to $\varepsilon_{\ddot{r}}$ and $\varepsilon_{\dot{c}}$. The phase perturbation should not exceed π radians over L_{syn} if the image is not to be defocused. This implies the following constraint:

$$|c_2 L_{syn}^2| < \pi \tag{20}$$

Based on the MASAR specifications, the allowable errors across the synthetic length are about 5 m for cross-track and vertical motions, and 0.4 m for along-track motions. The need for accurate motion measurement and proper motion compensation is apparent. In MASAR, the motion measurement is provided by the BEI Systron Donner C-MIGITS III integrated INS-GPS system. The update rate of the INS (inertial navigation system) and the GPS (global positioning system) are, respectively, 100 Hz and 1 Hz. The outputs are interpolated to reconstruct the motion trajectory in cross-range domain. The displacement of the antenna phase center from the ideal trajectory is estimated. Next, the projected slant range is computed and applied in (7) to yield an estimation of the phase error, $\hat{\phi}_e(y)$. The motion compensation is performed on the measured SAR signal in the (ω, y) domain via

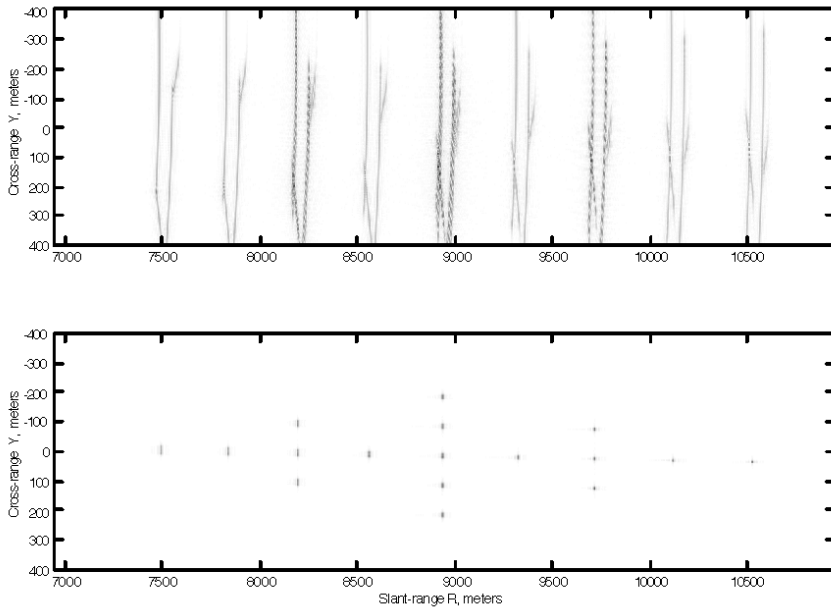$$\hat{S}(\omega, y) = S_e(\omega, y)e^{-j\hat{\phi}_e(y)} \tag{21}$$

Figure 8. The MASAR image before and after motion compensation.

There are other types of phase errors such as high-frequency sinusoidal phase errors due to vibration of antenna phase center, and wideband random errors caused by random noise. The former will cause spurious targets (high sidelobes) while the later decease signal-to-noise ratio in the SAR image. Their effects have been studied and discussed in [18]. In order to analyze the effect of trajectory deviations, seventeen point targets placed at arbitrary locations are used as a standard test site for MASAR. Fig. 8 shows the SAR image before and after motion compensation.

5. CONCLUSIONS

This paper describes the design and development of the MASAR system, which is targeted to be operational in Forth Quarter of 2006. Various system parameters have been carefully studied and selected in the high-level system design before actual hardware implementation. The patch antenna, radar electronics and high-speed SAR processing system have been constructed and tested in-house. The full integration of MASAR is an on-going activity, which focuses on the overall system

performance. The next step of the work is to mount the SAR system onto an aircraft for flight commissioning and actual field measurements.

ACKNOWLEDGMENT

REFERENCES

1. Skolnik, M. I., *Radar Handbook*, McGraw-Hill, New York, 1970.
2. Ulaby, F. T., R. K. Moore, and A. K. Fung, *Microwave Remote Sensing: Active and Passive*, Vol. 1, Artech House, Norwood, 1981.
3. Chan, Y. K., M. K. Azlindawaty, V. Gobi, B. K. Chung, and H. T. Chuah, "The design and development of airborne synthetic aperture radar," *Proc. IGRASS 2000*, Vol. 2, 518–520, July 2000.
4. *International Telecommunication Union's (ITU) World Radiocommunication Conference 1997 (WRC-97)*.
5. Ulaby, F. T. and M. C. Dobson, *Handbook of Radar Scattering Statistics for Terrain*, Artech House, Norwood, 1989.
6. Wiley, C. A. "Synthetic aperture radar—A paradigm for technology evolution," *IEEE Trans. Aerospace Elec. Sys.*, Vol. 21, 440–443, 1985.
7. Holtzman, J. C., V. S. Frost, J. L. Abott, and V. H. Kaupp, "Radar image simulation," *IEEE Trans. Geosci. Remote Sensing*, Vol. 16, No. 4, 296–303, 1978.
8. Dente, F. and F. Vinelli, "A model and a software tool for SAR product and system simulation: Practical application examples," *Proc. IGARSS '92*, 94–96, Texas, USA, 1992.
9. Franceschetti, G., M. Miglaccio, D. Riccio, and G. Schirinzi, "SARAS: A SAR raw signal simulator," *IEEE Trans. Geosci. Remote Sensing*, Vol. 30, No. 1, 110–123, 1992.
10. Christensen, E. L. and M. Dich, "SAR antenna design for ambiguity and multipath suppression," *Proc. IGARSS '3*, Vol. 2, 784–787, 1993.
11. Balanis, C. A., *Antenna Theory, Analysis and Design*, John Wiley & Sons, New York, 1997.
12. Hansen, R. C., *Phased Array Antennas*, John Wiley & Sons, New York, 1997.

13. Chan, Y. K., B. K. Chung, and H. T. Chuah, "Transmitter and receiver design of an experimental airborne synthetic aperture radar sensor," *Journal of Electromagnetic Waves and Applications*, (accepted for publication).

14. Gabor, D., "A new microscope principle," *Nature*, Vol. 161, 777, 1948.

15. Goodman, J., *Introduction to Fourier Optics*, McGraw-Hill, New York, 1968.

16. Soumekh, M., *Synthetic Aperture Radar Signal Processing with Matlab Algorithms*, John Wiley & Sons, Inc., 1999.

17. Kaith, R., "Synthetic aperture imaging radar and moving targets," *IEEE Trans. Aerospace Elec. Sys.*, Vol. 7, No. 3, 499–505, 1971.

18. Koo, V. C., T. S. Lim, M. C. Rao, and H. T. Chuah, "A GA-based autofocus technique for correcting high-frequency SAR phase error," *Journal of Electromagnetic Waves and Applications*, Vol. 8, No. 6, 781–795, 2004.

V. C. Koo received the B.Eng. (Hons) in Electrical Engineering from the University of Malaysia, in 1997 and the M.Eng.Sc. in Electrical Engineering from the Multimedia University, in 1999. He is presently a lecturer with the Faculty of Engineering and Technology, Multimedia University. His research interests include microwave remote sensing and radar technology. He is currently involved in the development of an airborne SAR system for remote sensing applications.

Y. K. Chan obtained his B.Eng. (Hons) in Electrical Engineering from the University of Malaya, in 1998 and M.Eng.Sc. in Electrical Engineering from the Multimedia University, in 2002. He is presently a lecturer with the Faculty of Engineering and Technology, Multimedia University. He involved in the development of an airborne SAR system for remote sensing applications since 1998. His research interests include microwave remote sensing, radar technology and RF circuit design.

G. Vetharatnam obtained his B.E. (Hons) in Electrical Engineering from University of Malaya, in 1998 and M.Eng.Sc. in Electrical Engineering from the Multimedia University, in 2003. He is presently a lecturer with the Faculty of Engineering, Multimedia University. His research interests include microwave remote sensing, microstrip antennas and radar technology.

T. S. Lim received the B.Eng. (Hons) and M.Eng.Sc. in Electrical Engineering from the University Technology of Malaysia, in 1998 and 2001. He is presently a lecturer with the Faculty of Engineering and Technology, Multimedia University. His research interests include microwave remote sensing, digital signal processing and radar technology. He is currently involved in the development of an airborne SAR system for remote sensing applications.

B. K. Chung graduated with a B.Eng. (Hons) in Electrical Engineering from the University of Malaya in 1992. He worked in the Design Department of Sony Electronics in Penang, Malaysia from 1992 to 1995. He then returned to the University of Malaya to undertake a research project and obtained his M.Eng.Sc. degree in Electrical Engineering in 1997. He obtained his Ph.D. in Microwave Engineering from Multimedia University in 2003. He is currently a senior lecturer at Multimedia University. His research interests includes microwave theory and techniques, radar, wireless communication systems, antenna design, remote sensing, electromagnetic compatibility, and electronic instrumentation and measurements.

H. T. Chuah obtained his B.Eng., M.Eng.Sc., and Ph.D., all in Electrical Engineering from the University of Malaysia. He is currently a Professor with the Faculty of Engineering, Multimedia University. Chuah was the recipient of the inaugural Young Engineer Award by the Institution of Engineers, Malaysia in 1991, the Young Scientist Award by Union of Radio Science to attend its 23rd and 24th General Assembly in Czechoslovakia and in Japan, respectively. He received the National Young Scientist Award (Industrial Sector) by the Malaysian Ministry of Science, Technology and Environment in 1995 and the Malaysian Toray Science and Technology Award in 1999. His research interests are in applied electromagnetic, microwave remote sensing and device physics.